

Sub shot-noise interferometry from measurements of the one-body density

J Chwedeńczuk¹, P Hyllus², F Piazza³ and A Smerzi^{4,5}

¹Faculty of Physics, University of Warsaw, ul. Hoża 69, 00-681 Warsaw, Poland

²Department of Theoretical Physics, University of the Basque Country UPV/EHU, P.O. Box 644, E-48080 Bilbao, Spain

³Physik Department, Technische Universität München, 85747 Garching, Germany

⁴INO-CNR and LENS, 50125 Firenze, Italy

⁵INO-CNR BEC Center and Dipartimento di Fisica, Università di Trento, 38123 Povo, Italy

Abstract. We derive the asymptotic maximum-likelihood phase estimation uncertainty for any interferometric protocol where the positions of the probe particles are measured to infer the phase, but where correlations between the particles are not accessible. First, we apply our formula to the estimation of the phase acquired in the Mach-Zehnder interferometer and recover the well-know momentum formula for the phase sensitivity. Then, we apply our results to interferometers with two spatially separated modes, which could be implemented with a Bose-Einstein condensate trapped in a double-well potential. We show that in a simple protocol which estimates the phase from an interference pattern a sub shot-noise phase uncertainty of up to $\Delta\theta \propto N^{-2/3}$ can be achieved. One important property of this estimation protocol is that its sensitivity does not depend on the value of the phase θ , contrary to the sensitivity given by the momentum formula for the Mach-Zehnder transformation. Finally, we study the experimental implementation of the above protocol in detail, by numerically simulating the full statistics as well as by considering the main sources of detection noise, and argue that the shot-noise limit could be surpassed with current technology.

1. Introduction

Quantum interferometry, a rapidly developing branch of modern physics, exploits some striking features of quantum mechanics in order to build ultraprecise measuring devices [1]. It employs non-classical states of light [2, 3, 4, 5] or matter [6, 7, 8, 9, 10, 11, 12] to beat the shot-noise limit (SNL) $\Delta\theta = 1/\sqrt{N}$ – the limit of precision of parameter estimation of a phase shift θ set by classical physics. Here N is the number of particles in the probe state. Recent achievements in the preparation of entangled states of atoms have put atomic interferometry [13] in the *avant-garde* for precise determination of electromagnetic [14, 15, 16] and gravitational [17, 18, 19] interactions.

A paradigmatic example and benchmark for every interferometer is the Mach-Zehnder interferometer (MZI), where two “beams” propagating along separated paths accumulate a relative phase θ (to be estimated) and are subsequently recombined through a beam splitter. A similar protocol which uses internal states instead of separate paths is known as Ramsey-spectroscopy [20]. It has been recently realized with a Bose-Einstein condensate (BEC), employing two hyperfine states of the atoms [9]. The beam-splitter was mimicked by coupling the two modes with a micro-wave pulse for a precisely chosen amount of time. Atomic interferometers with spatially separated modes, which could for instance be used to measure forces decaying with the distance are more challenging in implementation due to the difficulty of performing the beam-splitter transformation [21, 22].

In this paper we consider a simple “double-slit” interferometer in which two beams are recombined through a free expansion of two initially localized clouds with the output signal obtained by measuring the positions of the particles. After preparation of a suitably entangled input state, sub shot-noise (SSN) interferometry requires thus refined particle detection at the output. Some new techniques of atom-position measurements, like the micro-channel plate [23], the tapered fiber [24], the light-sheet method [25] or techniques involving atomic fluorescence from the lattice [26], give hope for an almost 100% efficient single-atom detection in the nearby future. Such a tool in principle could even give access to atom-atom correlations at all orders.

It has been shown [27, 28] that the measurement of the N -th order correlation function is the best possible estimation strategy for inferring the phase between two interfering BEC wave-packets, and allows to reach the Heisenberg limit of phase uncertainty. However, even with small BECs, the measurement of the N -th order correlation function would require substantial experimental effort, since a huge configurational space must be probed with sufficient signal to noise ratio.

The difficulty of measuring high order correlation functions is the motivation for this work. We show that by measuring positions of particles the phase can be estimated with a SSN phase uncertainty using the simple one-body density. We consider two possible detection scenarios: the output signal consists of (a) the positions of single atoms, or (b) the number of atoms per pixel, which corresponds to the commonly employed least-squares estimation from the fit to the average density [29]. For both cases, we compute

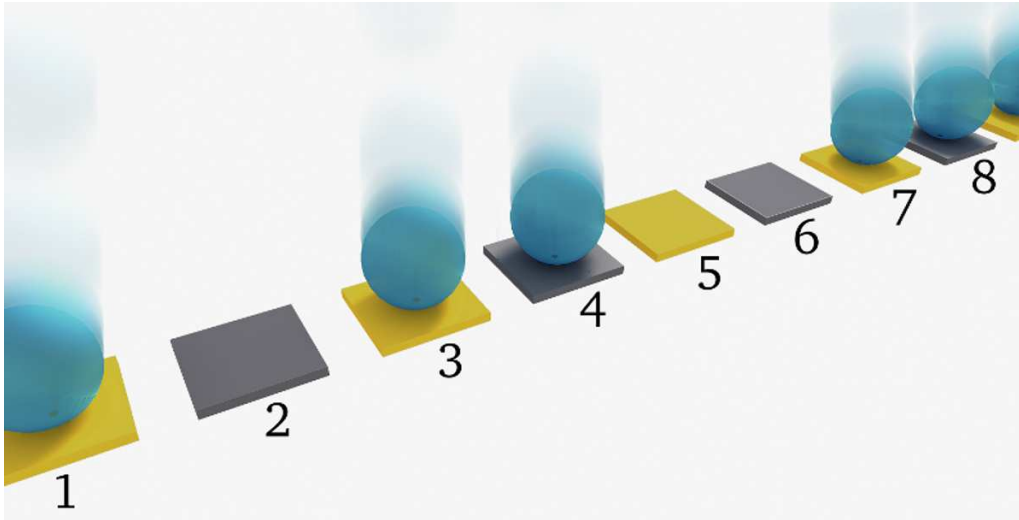


Figure 1. Schematic representation of the atom position measurement, where the detectors (boxes) turn yellow (no. 1, 3 and 7) when they are hit by atoms (spheres). Some detectors however remain gray (as the detector no. 8), so the detection efficiency drops, and sometimes a neighbouring box turns yellow (no. 5 instead of no. 4), which limits the spatial resolution.

the general asymptotic phase uncertainty of a maximum-likelihood phase estimation scheme using the one-body density only.

We verify that in an MZI situation, estimating the phase from the one-body density is equivalent to estimation from the average population imbalance between the arms of the interferometer, and recover the known result that the sensitivity can saturate the Heisenberg limit.

We then apply this estimation protocol to our case of interest, namely, two interfering BEC wavepackets. We provide an analytical expression for the phase uncertainty which shows SSN scaling with phase squeezed states in input. Contrary to the MZI, the phase uncertainty does not depend on the phase θ , which could be an important advantage. We then analyze the full statistics of the phase estimation by numerically simulating experiments with a realistic number of particles. We find that already small statistical samples are sufficient to saturate the analytical asymptotic prediction for the phase uncertainty. Finally, we discuss the main sources of noise affecting the interferometric precision, which we expect to concern the atom detection stage. We argue that including the effect of imperfect detection the SNL can still be surpassed, and that the necessary amount of squeezing could be achieved in a realistic double-well setup.

The paper is organized as follows. In Section 2 we derive the general expression for the uncertainty of the phase estimated from the one-body density. We consider two possible detection scenarios. We assume either having access to positions of single particles or a coarse grained measurement due to a limited detection capability. In Section 3, we apply the above results to the case of the MZI. In Section 4 we turn to

our case study where the interferometer consists of a simple phase-imprint between the modes followed by the ballistic expansion of the mode functions. We also show how the phase uncertainty for the phase estimation from the density of the interference pattern is influenced by characteristic sources of noise. Some details of analytical calculations are presented in the Appendices.

2. Sensitivity of the one-body density estimator

An interferometric estimation protocol can be divided in: (i) the interferometer transformation, (ii) the measurement at the output, and (iii) the phase inference through an estimator. In (i), the interferometer imprints a relative phase θ on the N -particle input state $|\psi_{\text{in}}\rangle$. Such transformation can be represented by a unitary evolution operator $\hat{U}(\theta) = e^{i\theta\hat{h}}$, where \hat{h} is linear – i.e. can be written as a sum of operators acting on each particle separately – and does not depend on θ . In the Heisenberg picture, the field operator evolves as $\hat{\Psi}(x|\theta) \equiv \hat{U}^\dagger(\theta)\hat{\Psi}(x)\hat{U}(\theta)$ and $|\psi_{\text{in}}\rangle$ is unchanged. In the following, we will specify our arguments to the case of particle position measurements at the output, although the results of Sec. 2.1 are valid in general. We will thus consider next that in stage (ii), upon leaving the interferometer, the positions of the particles are detected. As observed above, due to the difficulty of obtaining high order correlation functions, often only the lowest, namely the density, can be precisely measured. This density, when normalized, gives

$$p_1(x|\theta) = \frac{\langle \hat{\Psi}^\dagger(x|\theta)\hat{\Psi}(x|\theta) \rangle}{N}, \quad (1)$$

the probability density of measuring a single particle at position x given θ . The average value is calculated for the input state $|\psi_{\text{in}}\rangle$. Next, we assume having no access to the correlations, so the phase is inferred only using $p_1(x|\theta)$ and the measurement outcomes obtained in stage (ii).

2.1. Single-atom detection

When in (ii) single-atom detection is performed, see Fig. 1, each experiment gives the positions of the N atoms, $\vec{x}_N^{(i)} = x_1^{(i)}, \dots, x_N^{(i)}$, where the label $i = 1, \dots, m$ indicates the particular iteration of the experiment. The accumulated set of data, N times m positions, is used to construct the likelihood function,

$$\mathcal{L}(\varphi) = \prod_{i=1}^m \prod_{k=1}^N p_1(x_k^{(i)}|\varphi). \quad (2)$$

The prescription of the Maximum Likelihood Estimator (MLE) is to infer the phase $\theta_{\text{ML}}^{(m)}$ in stage (iii) as the value of φ which maximizes Eq. (2). As demonstrated in the Appendix A, this MLE is consistent, i.e. $\theta_{\text{ML}}^{(m)} \rightarrow \theta$ for $m \rightarrow \infty$. There, we also obtain the uncertainty of the estimator equal to

$$\Delta^2 \theta_{\text{ML}}^{(m)} = \frac{1}{m} \frac{1}{NF_1} \left(1 + (N-1) \frac{C}{F_1} \right), \quad (3)$$

where C depends on the two-body probability density of detecting one particle at x_1 and the other at x_2 ,

$$p_2(x_1, x_2|\theta) = \frac{\langle \hat{\Psi}^\dagger(x_1|\theta) \hat{\Psi}^\dagger(x_2|\theta) \hat{\Psi}(x_2|\theta) \hat{\Psi}(x_1|\theta) \rangle}{N(N-1)}, \quad (4)$$

and reads [30]

$$C = \int dx_1 dx_2 p_2(x_1, x_2|\theta) \frac{\partial_\theta p_1(x_1|\theta)}{p_1(x_1|\theta)} \frac{\partial_\theta p_1(x_2|\theta)}{p_1(x_2|\theta)}. \quad (5)$$

Furthermore F_1 is the Fisher information calculated with the probability p_1 ,

$$F_1 = \int dx \frac{[\partial_\theta p_1(x|\theta)]^2}{p_1(x|\theta)}. \quad (6)$$

Equation (3) is the first important result of this paper. The phase, which is estimated from the single-body probability, depends on both p_1 and p_2 . If $C = 0$ or neglected as in [27], Eq. (3) provides a shot-noise limited phase uncertainty, since $F_1 \leq 1$ [27]. Yet, C can assume negative values, allowing for SSN phase uncertainty, as will be demonstrated below.

We also underline the generality of the above result, which is valid for any quantum state, where the parameter θ is estimated from the one-body density. In analogy, if two-body correlations can be measured in an experiment, four-body correlations would enter in the corresponding expression for the asymptotic phase uncertainty.

2.2. Multiple-atom detection

It is also important to consider the possibility that the detectors cannot resolve positions of individual particles. In this case, we need to use the coarse-grained density and assume that in stage (ii) in the i -th experiment the number of atoms $n_k^{(i)}$ in each of the $k = 1 \dots n_{\text{bin}}$ bins is measured (the bin size Δx must be small to precisely sample the density variations). The measurement is repeated m times and the phase is estimated from a least square fit of the one-body density to the accumulated data. As discussed in detail in [29], the phase uncertainty of such fit is equivalent to the phase uncertainty of the MLE with the likelihood function $\mathcal{L}_{\text{fit}}(\varphi) = \prod_{k=1}^{n_{\text{bin}}} p(\bar{n}_k|\varphi)$, where $p(\bar{n}_k|\varphi)$ is the probability for detecting $\bar{n}_k = \frac{1}{m} \sum_{i=1}^m n_k^{(i)}$ atoms on average in the k -th bin. For large m , according to the Central Limit Theorem, the probability $p(\bar{n}_k|\varphi)$ is a Gaussian with a mean $\langle n_k \rangle = \Delta x N p_1(x_k|\varphi)$ and Poissonian fluctuations, $\Delta^2 n_k = \langle n_k \rangle$ [27]. For the phase uncertainty of this MLE, we obtain similarly as in Section 2.1 that

$$\Delta^2 \theta_{\text{fit}}^{(m)} = \frac{\sum_{k=1}^{n_{\text{bin}}} \frac{[\partial_\theta \langle n_k \rangle]^2}{\langle n_k \rangle} + \sum_{k \neq l=1}^{n_{\text{bin}}} \sigma_{k,l}^2 \frac{\partial_\theta \langle n_k \rangle}{\langle n_k \rangle} \frac{\partial_\theta \langle n_l \rangle}{\langle n_l \rangle}}{m \left[\sum_{k=1}^{n_{\text{bin}}} \frac{[\partial_\theta \langle n_k \rangle]^2}{\langle n_k \rangle} \right]^2}, \quad (7)$$

where

$$\sigma_{k,l}^2 = (\Delta x)^2 N [(N-1)p_2(x_k, x_l|\theta) - N p_1(x_k|\theta)p_1(x_l|\theta)].$$

In the continuous limit $\Delta x \rightarrow 0$, the formulas (3) and (7) coincide.

3. Estimation from the one-body density with the MZI

As a benchmark for the phase estimation protocol introduced in Sec. 2, we first consider the case where in stage (i) the system acquires the phase θ in a MZI. The interferometric sequence of the MZI consists of three steps. First, the initial two-mode state $|\psi_{\text{in}}\rangle$ passes a beam-splitter. Then, a relative phase θ is imprinted between the modes. In the final stage of the interferometer, another beam-splitter acts on the state.

It can be easily shown that the evolution operator of the whole MZI sequence is $\hat{U}(\theta) = e^{-i\theta\hat{J}_y}$ [31]. It is convenient to switch to the Heisenberg picture. The initial field operator reads $\hat{\Psi}(x) = \psi_a(x)\hat{a} + \psi_b(x)\hat{b}$, where \hat{a}/\hat{b} annihilates a particle from mode a/b and the corresponding spatial mode function is $\psi_{a/b}(x)$. When passing the MZI, this operator is transformed as follows

$$\hat{\Psi}(\theta) = e^{i\theta\hat{J}_y}\hat{\Psi}(x)e^{-i\theta\hat{J}_y} = \psi_a(x) \left[\hat{a} \cos \frac{\theta}{2} - \hat{b} \sin \frac{\theta}{2} \right] + \psi_b(x) \left[\hat{b} \cos \frac{\theta}{2} + \hat{a} \sin \frac{\theta}{2} \right]. \quad (8)$$

We use this result to calculate the one-body [cf. Eq. (1)] and two-body [cf. Eq. (4)] probability densities that enter Eq. (3), assuming that both the mode functions are point-like and trapped in separate arms of the interferometer, i.e. $\psi_a(x)\psi_b(x) = 0$ for all x . Using an initial N -particle two-mode state $|\psi_{\text{in}}\rangle = \sum_j c_j |j, N-j\rangle$, where $|c_j|^2$ is the probability of having j atoms in mode a and $(N-j)$ in b , we get

$$\Delta^2\theta_{\text{ML}}^{(m)} = \frac{1}{m} \frac{\Delta^2\hat{J}_z \cos^2\theta + \Delta^2\hat{J}_x \sin^2\theta}{\langle \hat{J}_x \rangle^2 \cos^2\theta}. \quad (9)$$

The details of the derivation are presented in Appendix B. The above expression coincides with the phase uncertainty for the estimation of the phase θ from the average population imbalance between the two arms of the MZI. This coincidence can be explained as follows. When atoms are trapped in two separate arms of the interferometer, their positions can be directly translated to the number of particles in each arm, without any loss of information. It is then not surprising that the estimators basing on the average population imbalance and the average density are equivalent.

Note that for a particular case of $\theta = 0$, we get

$$\Delta^2\theta_{\text{ML}}^{(m)} = \frac{1}{mN} \xi_n^2, \quad (10)$$

where $\xi_n = \sqrt{N \frac{\Delta^2\hat{J}_z}{\langle \hat{J}_x \rangle^2}}$ is the spin-squeezing parameter [20, 32] related to number squeezing of the initial state. The expression (10) can provide up to the Heisenberg scaling of the phase uncertainty, once the interferometer is fed with a strongly number-squeezed state [33].

4. Estimation from the one-body density with the interference pattern

We now turn the attention to our case of interest, to which we devote the rest of the manuscript. We consider the whole phase acquisition sequence as consisting of two

steps. First is the phase-imprint performed in absence of two-body interactions, which in the two-mode picture is represented by the unitary operator $e^{-i\theta\hat{J}_z}$, and gives

$$\hat{\Psi}(x|\theta) = \psi_a(x)e^{i\frac{\theta}{2}}\hat{a} + \psi_b(x)e^{-i\frac{\theta}{2}}\hat{b}. \quad (11)$$

Then, the trap is opened. Since the two-body collisions are assumed to be not present, the two wave-packets freely spread and interfere. Atom interactions can strongly influence the expansion at an early stage, when the density of the clouds is high [34, 35]. We assume that initially $\psi_{a/b}(x)$ have identical shape, but are centered around $\pm x_0$. After long expansion time (in the so-called ‘‘far field’’) $\psi_{a/b}(x) \simeq e^{\mp i\frac{\kappa x}{2}} \cdot \tilde{\psi}\left(\frac{x}{\tilde{\sigma}^2}\right)$, where $\tilde{\sigma} = \sqrt{\frac{\hbar t}{\mu}}$ (μ is the atomic mass and t is the expansion time) and $\kappa = 2\frac{x_0}{\tilde{\sigma}^2}$, $\tilde{\psi}$ is the Fourier transform of the wave-packets at $t = 0$, the same for $\psi_{a/b}$ [27, 28]. Note that we have dropped the common factor $e^{i\frac{x^2}{2\tilde{\sigma}^2}}$. Some aspect of this simple interferometric sequence, which does not require the implementation of a beam splitter, have been discussed in [28].

The field operator $\hat{\Psi}(x|\theta)$ gives $p_1(x_1|\theta)$ and $p_2(x_1, x_2|\theta)$ presented in the Appendix C, which are put into Eq. (3). The integrals are performed analytically assuming that the interference pattern consists of many fringes, giving

$$\Delta^2\theta_{\text{ML}}^{(m)} = \frac{1}{mN} \left[\xi_\phi^2 + \frac{\sqrt{1 - \nu^2}}{\nu^2} \right], \quad (12)$$

where $\xi_\phi = \sqrt{N\frac{\Delta^2\hat{J}_y}{\langle\hat{J}_x\rangle^2}}$ is the spin-squeezing parameter [36] related to phase-squeezing of the initial state. Also, we have introduced $\nu = \frac{2}{N}\langle\hat{J}_x\rangle$ – i.e. the visibility of the interference fringes, see Eq. (C.1) and below for details. One important property of Eq. (12) is its independence of the actual value of the phase θ . This can be understood as follows. The probabilities (1) and (4) depend on θ in the same manner, i.e. via a sine or cosine function, see Eqs (C.1) and (C.2). Since the integration in (5) and (6) runs over the whole space, the shift of the trigonometric functions by a common factor θ is irrelevant, since within the envelope $\tilde{\psi}\left(\frac{x}{\tilde{\sigma}^2}\right)$ there are many interference fringes. On the other hand, the sensitivity of the MZI (9) depends on θ and has some optimal ‘‘working points’’ because the wave-packets $\psi_{a/b}(x)$ do not add up to a wide envelope and therefore the argument for θ -independence valid for the interference pattern does not apply here. Therefore, the θ -independence of Eq. (12) might be an advantage of this estimation protocol with respect to the momentum formula of the MZI, valid when the phase is estimated from the one-body density.

Note that the phase uncertainty of the MZI [Eq. (10)] would closely resemble the above result if the second term of Eq. (12) were absent. In the former case, $\Delta^2\theta_{\text{ML}}^{(m)}$ benefits from the number-squeezing because the estimator is equivalent to the average population imbalance between the arms of the interferometer, therefore a state with reduced population imbalance fluctuations decreases the uncertainty $\Delta^2\theta_{\text{ML}}^{(m)}$. Analogously, in the latter case, the decreasing fluctuations of the relative phase between the two modes would improve the estimation precision.

However, the situation complicates due to the presence of the second term in Eq. (12). Namely, when ξ_ϕ drops, so does the fringe visibility ν and so the amount of information about the phase θ contained in the one-body density degrades. As a consequence, the phase uncertainty of the estimation from $p_1(x|\theta)$ declines.

It is now important to check whether, due to this interplay between improvement from the phase-squeezing and deterioration from the loss of visibility, Eq. (12) can give SSN phase uncertainty at all. To this end, we calculate $\Delta^2\theta_{\text{ML}}^{(m)}$ with phase-squeezed states for $N = 100$, which we generate by computing the ground state of the two-mode Hamiltonian $\hat{H} = -\hat{J}_x + \frac{U}{NJ}\hat{J}_z^2$ for negative values of the interaction-to-tunnelling ratio $\frac{U}{NJ}$. For a detailed study of the preparation of phase-squeezed states, including experimental sources of noise, see [36]. For every value $\frac{U}{NJ}$, we find $|\psi_{\text{in}}\rangle$ and calculate ξ_ϕ and ν . These values are substituted into Eq. (12) and the resulting $\Delta^2\theta_{\text{ML}}^{(m)}$ is plotted in Fig. 2 as a function of ξ_ϕ .

Clearly, the uncertainty drops below the SNL. We notice the presence of an optimal

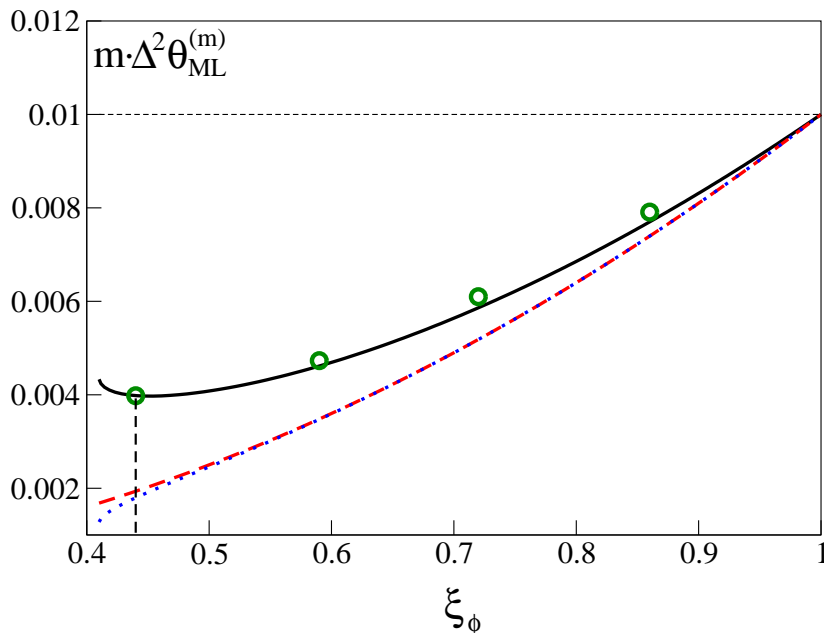


Figure 2. The phase uncertainty (12) – black solid line – as a function of ξ_ϕ for $N = 100$ particles. The dashed red line is the phase uncertainty from the squeezing parameter (in absence of the second term in Eq. (12)), while the dotted blue line is given by the inverse of the QFI. The horizontal dashed line denotes the SNL and the vertical dashed line indicates the position of the optimal point. The open green circles are the result of a numerical experiment (see text) for four values of $\xi_\phi = 0.44, 0.59, 0.72$ and 0.86 with $m = 10, n_{\text{rep}} = 4000$.

point, where the gain from the spin-squeezing is balanced by the loss of visibility. The figure also shows that the phase uncertainty (12) does not saturate the bound set by the Quantum Fisher Information (QFI), $\Delta^2\theta_{\text{QFI}} \equiv \frac{1}{m} \frac{1}{F_Q} = \frac{1}{m} \frac{1}{4\Delta^2 J_z}$ [37].

To support these analytical results for the asymptotics, we also study the full statistics of the protocol by simulating a phase-estimation experiment with $N = 100$

particles. We generate the input state with a desired amount of phase-squeezing, evaluate the full N -body probability $p_N(\vec{x}_N|\theta)$, with which we draw a single realization yielding the N positions. We repeat the experiment m times and obtain one value of the phase $\theta_{\text{ML}}^{(m)}$ using MLE with Eq. (2). This cycle is performed n_{rep} times and the variance of the estimator is calculated on the resulting ensemble. The results, plotted (empty circles) in Fig. 2 for four values of ξ_ϕ , $m = 10$, and $n_{\text{rep}} = 4000$, agree with the theoretical value calculated with Eq. (12). An important information in view of an experimental implementation is that though formally the MLE saturates (12) when $m \rightarrow \infty$, in practice $m = 10$ is sufficient to reach the bound, as shown in the upper panel of Fig. 3. The lower panel of Fig. 3 shows instead the average value of the estimated phase plus uncertainties as a function of m . Here we have chosen the true value of θ to be zero, thus the figure shows that the estimator is unbiased.

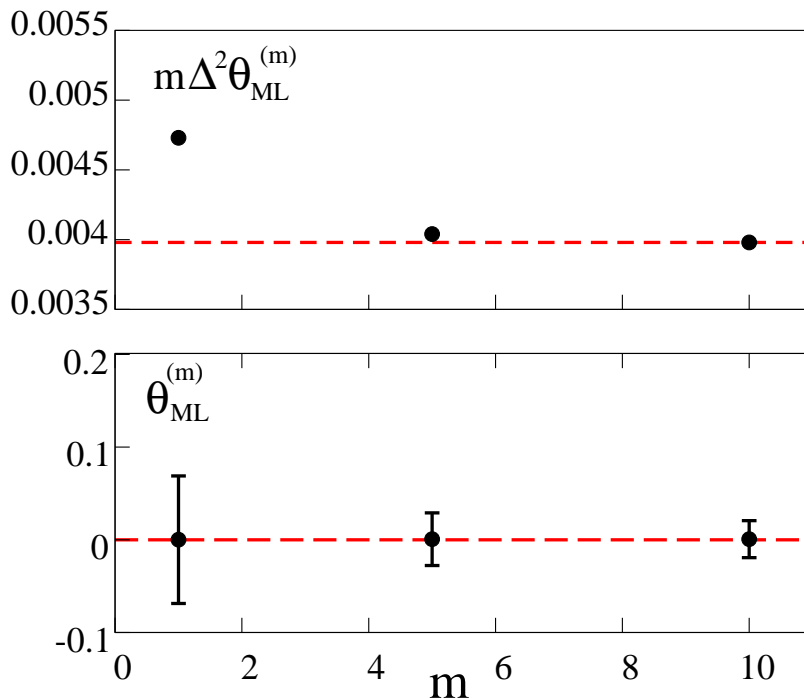


Figure 3. The upper panel shows that the phase uncertainty of the “experiment” (black points) at the optimal point $\xi_\phi = 0.44$ and $N = 100$ beats the SNL (which is equal to $m\Delta^2\theta_{\text{ML}}^{(m)} = 0.01$ here, cf. Fig. 2) already for $m = 1$ and converges to the theoretical value (dashed red line) for $m = 10$. The lower panel depicts the corresponding average plus error bars indicating uncertainties, while the true value of θ is indicated by the dashed red line.

Our next step is to find the best scaling of Eq. (12) with N . In order to get an analytical estimate, we model $|\psi_{\text{in}}\rangle$ with a Gaussian, see Appendix D, and find that at the optimal point $m\Delta^2\theta_{\text{ML}}^{(m),\text{opt}} = 2N^{-4/3}$. This prediction is compared with numerical results, where for every N we evaluate the phase uncertainty (12) at the optimal state. As shown in the inset of the Fig. 4, the agreement between the numerics and the Gaussian approximation is very good. Also, we numerically obtain the scaling of the

QFI at the optimal state $m\Delta^2\theta_{\text{QFI}}^{\text{opt}} = N^{-4/3}$, which differs from $\Delta^2\theta_{\text{ML}}^{(m),\text{opt}}$ just by a factor of 2. Next, we discuss some characteristic experimental imperfections which can spoil the phase uncertainty (12).

4.1. Impact of detection imperfections

Single-particle detection, which is the basis of the estimation scheme discussed in Sec. 2.1, is affected by two dominant sources of noise: limited efficiency and finite spatial resolution, see Fig. 1. The former is incorporated by letting the index k run from 1 to $n < N$ in Eq. (2). In effect, n replaces N in Eq. (3). The finite spatial resolution modifies instead both C and F_1 . We implement it by convoluting the probabilities $p_1(x_1|\theta)$ and $p_2(x_1, x_2|\theta)$ with $\tilde{p}(x_1|x'_1) = \frac{1}{\sqrt{2\pi\sigma^2}}e^{-(x_1-x'_1)^2/(2\sigma^2)}$ (and analogously for x_2) – a Gaussian probability of detecting an atom at x_1 given its true position x'_1 . The convolutions are calculated analytically and the phase uncertainty becomes

$$\Delta^2\tilde{\theta}_{\text{ML}}^{(m)} = \frac{1}{mN} \left[\xi_\phi^2 + \frac{\left(\sqrt{1 - \nu^2 e^{-\kappa^2\sigma^2}} + 1\right) e^{\kappa^2\sigma^2} - \eta}{\eta\nu^2} \right], \quad (13)$$

where $\kappa = \frac{2x_0}{\sigma^2}$ and $\tilde{\sigma} = \sqrt{\frac{\hbar t}{\mu}}$ were defined below Eq. (11). Above, we assumed that $N, n \gg 1$, $\eta = \frac{n}{N}$ and the tilde denotes the phase uncertainty in presence of errors. Note that for $\eta = 100\%$ and $\sigma = 0$ we recover Eq. (12). In Fig. 4 we plot Eq. (13) as a function of σ for $N = 100$ and $\eta = 100\%, 90\%, 80\%$ and 70% . For instance, with resolution of 1/30-th of a fringe ($\sigma = 0.033 \times \frac{2\pi}{\kappa} \simeq \frac{0.2}{\kappa}$) and $\eta = 90\%$, the SSN scaling is $m\Delta^2\tilde{\theta}_{\text{ML}}^{(m),\text{opt}} = 1.48N^{-1.16}$, shown in the inset. Also note that even in presence of the noise, the phase uncertainty (13) does not depend on θ .

The two main sources of detection noise affecting the least-squares fit estimation protocol defined in Sec. 2.2, not shown in Fig. 1, are imperfect atom counting and the finite bin size. To model the former, we assume that the number of atoms in each bin is measured with some uncertainty, and convolute the probabilities entering the fit likelihood function with a Gaussian error distribution, $p_{\text{err}}(\bar{n}_k|\bar{n}'_k) = \frac{\sqrt{m}}{\sqrt{2\pi\sigma_{\text{err}}^2}}e^{-(\bar{n}_k-\bar{n}'_k)^2/(2\sigma_{\text{err}}^2/m)}$. As a result, the variance is increased by σ_{err}^2/m . Very promising detection techniques based on the detection of fluorescence photons rely upon detection of on average α fluorescence photons per atom, and this number fluctuates at the shot noise level. Error propagation gives $\sigma_{\text{err}}^2 = \frac{1}{\alpha}\langle n_k \rangle$ and the phase uncertainty (7) becomes

$$\Delta^2\tilde{\theta}_{\text{fit}}^{(m)} = \Delta^2\theta_{\text{fit}}^{(m)} + \frac{1}{m} \frac{1}{\alpha} \frac{1}{\sum_{k=1}^{n_{\text{bin}}} \frac{[\partial_\theta \langle n_k \rangle]^2}{\langle n_k \rangle}}.$$

Using $N = 100$ and the optimal state denoted by the vertical line in Fig. 2, for the bin size $\Delta x = \frac{0.2}{\kappa}$ a SSN phase uncertainty is preserved for $\alpha \gtrsim 2.2$ – a condition well satisfied by the light-sheet technique, which can give $\alpha \simeq 10$ photons per atom [25].

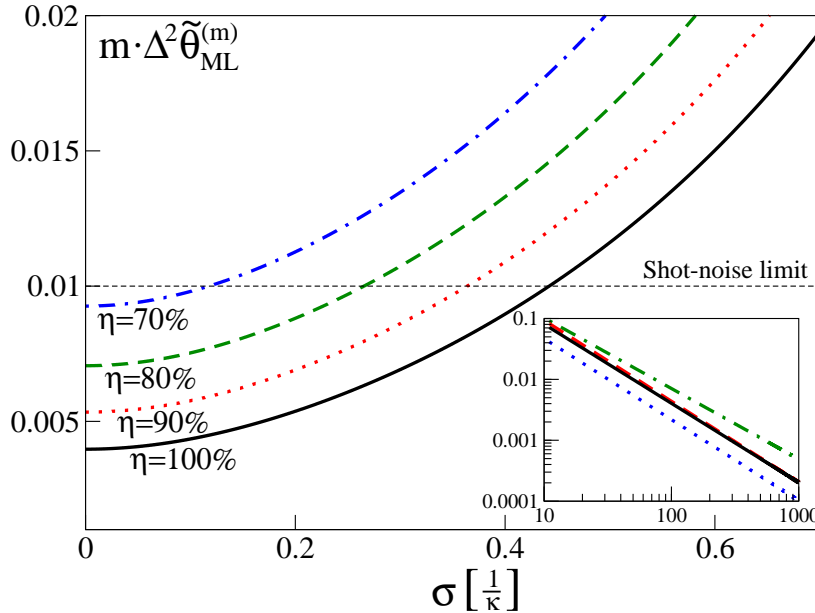


Figure 4. The phase uncertainty (13), calculated for $N = 100$ in the optimal state (denoted by the vertical dashed line in Fig. 2), as a function of σ for four different values of η . The horizontal dashed line denotes the SNL. The inset shows the phase uncertainty Eq. (12) as a function of N (solid black line) with the optimal state, compared to the scaling from the Gaussian approximation, $m\Delta^2\theta_{\text{ML}}^{(m),\text{opt}} = 2N^{-4/3}$ (dashed red line), the scaling of the QFI $m\Delta^2\theta_{\text{QFI}}^{(m),\text{opt}} = N^{-4/3}$ (dotted blue line) and the scaling of Eq. (13) with $\sigma = \frac{0.2}{\kappa}$ and $\eta = 90\%$, giving $m\Delta^2\tilde{\theta}_{\text{ML}}^{(m),\text{opt}} = 1.48N^{-1.16}$ (dash-dotted green line).

5. Conclusions

We have derived an expression for the phase estimation uncertainty for a generic situation where the phase is inferred from the positions of probe particles, when only the one-body density is known. In a Mach-Zehnder type interferometer, the sensitivity of this protocol coincides with the well known error propagation formula and we recover the known Heisenberg limited phase uncertainty, $\Delta\theta \propto N^{-1}$. Then we consider the simplest “double-slit” interferometer based on spatially interfering wave-packets suggested in Ref. [28], which still scales at best as $\Delta\theta \propto N^{-2/3}$, limited by the loss of fringe visibility. Nevertheless, the phase uncertainty for the interference pattern (12) has a major advantage over the MZI (9). Namely, it performs equally well for any value of θ , while (9) can reach very high values around $\theta = \frac{\pi}{2}$ and $\theta = \frac{3}{2}\pi$.

The interferometric protocol employing the interference pattern could be implemented with a BEC trapped in a double-well potential. After imprinting the phase and switching the trap off, the two clouds would expand and interfere. The atoms could then be detected using for instance the light-sheet method [25], based on the fluorescence measurement of photons scattered by the atoms crossing a laser beam. Another possible scheme relies upon letting the atoms fall onto an optical lattice. If the interference pattern is dilute so that there is no more than one atom per site, their

positions could be detected by a fluorescence measurement [26] with ultra-high efficiency and resolution. Recent quantum interferometry experiments [9, 11, 38] indicate that very important effects limiting the phase uncertainty are the detection imperfections, which we believe to have realistically taken into account in our proposal. Another relevant constraint to the precision of a double-well interferometer comes from the noise present in the interferometric sequence i). A recent theoretical work [36] shows that the amount of squeezing at the optimal point ($\xi_\phi = 0.44$ for $N = 100$ particles) could be reached with a double-well BEC using a refocusing method even in presence of the latter source of noise.

6. Acknowledgements

We gratefully acknowledge discussions with Julian Grond and Aurélien Perrin. We thank Baltazar Brukalski for preparing Fig.1. J. Ch. acknowledges Foundation for Polish Science International TEAM Program cofinanced by the EU European Regional Development Fund and the support of the National Science Center. P.H. acknowledges support from the ERC Starting Grant GEDENTQOPT and CHIST-ERA QUASAR. F.P. acknowledges support by the Alexander Von Humboldt foundation. A.S. acknowledges support of the EU-STREP Project QIBEC.

Appendix A. Derivation of the phase uncertainty

Appendix A.1. Single-atom detection

The proof that the estimator taken as the phase $\theta_{\text{ML}}^{(m)}$ which maximizes the likelihood function of Eq. (2) is unbiased and has the variance of Eq. (3) asymptotically in m can be performed along the lines of the standard proof that the Maximum-Likelihood method saturates the Cramér-Rao bound [39] for $m \gg 1$

$$\Delta^2 \theta_{\text{ML}}^{(m)} \geq \frac{1}{mF}, \quad (\text{A.1})$$

where F is the Fisher information to be defined below. The original proof was given in Ref. [39]. Recent formulation can be found in Ref. [40], and a more accessible albeit less rigorous version is given in Ref. [41].

The proof consists of two steps. Firstly, we show that the estimator is *consistent*, *i.e.*, for $m \rightarrow \infty$, the probability that $\theta_{\text{ML}}^{(m)} \neq \theta$ goes to zero, which means that the estimator approaches the true value of the phase shift asymptotically. This demonstration follows Ref. [40]. Secondly, we adapt the simplified proof of Ref. [41] (see also [39]) that a consistent ML estimator is also *efficient*, which means that it saturates the Cramér-Rao bound, Eq. (A.1), for $m \gg 1$. In particular, the proof shows that for large m , $\theta_{\text{ML}}^{(m)}$ is distributed with a Gaussian distribution with the variance of Eq. (2) and mean θ , hence it is also unbiased.

Before we start, a remark is in order. It might seem surprising or even wrong to use the likelihood function of Eq. (2). The reason is that we use only the single particle

probabilities to estimate the phase, even though in a single shot of the experiment, the N particles will be correlated in general. Hence the probability that in a single shot the second particle arrives at a position x_2 generally depends on the position x_1 where the first particle was detected. In traditional ML estimation, one would therefore define the likelihood function as

$$\mathcal{L}(\varphi) = \prod_{i=1}^m p_N(\vec{x}_N^{(i)}|\varphi) \quad (\text{A.2})$$

with the N -particle conditional probability density $p_N(\vec{x}_N|\varphi)$ instead and define the estimator as the maximum of this function. As mentioned above it can be shown [39, 40, 41] that this estimator is consistent, unbiased, and that it saturates the Cramer-Rao bound with the Fisher information

$$F_N = \int d\vec{x} \frac{1}{p_N(\vec{x}_N|\theta)} \left(\partial_\theta p_N(\vec{x}_N|\theta) \right)^2. \quad (\text{A.3})$$

This bound cannot be overcome by any other estimator using the results of the measurement governed by the probability density $p_N(\vec{x}_N|\theta)$ or by any of its reductions.

However, there are no restrictions on how an estimator can be defined, there will only be differences in the performance of different estimators. We define the estimator based on the single-particle probability density only. As the proof below shows, this estimator is consistent, unbiased, and has the variance of Eq. (2). The variance is ultimately limited (but is generally larger than) the ultimate limit from Eq. (A.1) with the Fisher information from Eq. (A.3). However, it has the advantage that it is accessible experimentally and also allows for sub shot-noise phase estimation, as shown in the main article.

Consistency. We recall the definition of $\theta_{\text{ML}}^{(m)}$, which is the value of the parameter φ which maximizes $\mathcal{L}(\varphi)$ from Eq. (1) from the main article. Equivalently, it maximizes

$$f^{(m)}(\varphi) \equiv \frac{1}{m} \sum_{i=1}^m \sum_{k=1}^N \ln p_1(x_k^{(i)}|\varphi), \quad (\text{A.4})$$

where N is the number of particles and m the number of independent repetitions of the experiment. The events \vec{x}_N are distributed with the conditional probability density $p_N(\vec{x}_N|\theta)$, where θ is the true value of the phase shift, and $p_1(x_k|\theta)$ is obtained from $p_N(\vec{x}_N|\theta)$ by integrating over all $x_{j \neq k}$.

We assume *identifiability*, *i.e.*, that $p_1(x|\theta) = p_1(x|\theta')$ for all x is equivalent to $\theta = \theta'$. Consistency is then proved by showing that $f(\varphi) = \lim_{m \rightarrow \infty} f^{(m)}(\varphi)$ has a maximum at $\varphi = \theta$ as follows:

$$\begin{aligned} f(\varphi) - f(\theta) &= \lim_{m \rightarrow \infty} \frac{1}{m} \sum_{i=1}^m \sum_{k=1}^N \left(\ln p_1(x_k^{(i)}|\varphi) - \ln p_1(x_k^{(i)}|\theta) \right) \\ &= \sum_{k=1}^N \int d\vec{x}_N p_1(x_k|\theta) \left(\ln p_1(x_k|\varphi) - \ln p_1(x_k|\theta) \right) \\ &= N \int dx p_1(x|\theta) \ln \frac{p_1(x|\varphi)}{p_1(x|\theta)} \leq 0, \end{aligned} \quad (\text{A.5})$$

where we have used $\ln(y) \leq y - 1$. The equality is obtained *iff* $y = 1$. Hence the inequality Eq. (A.5) is saturated *iff* $p_1(x|\varphi) = p_1(x|\theta)$ for all x . It follows that $\varphi = \theta$ by the identifiability assumption. Hence $\theta_{\text{ML}}^{(m)} \rightarrow \theta$ for $m \rightarrow \infty$.

Efficiency. We expand the first derivative of \mathcal{L} from Eq. (1) of the main article around θ ,

$$\partial_\varphi \log \mathcal{L}(\varphi) \simeq \partial_\varphi \log \mathcal{L}(\varphi)|_\theta + \partial_\varphi^2 \log \mathcal{L}(\varphi)|_\theta (\varphi - \theta). \quad (\text{A.6})$$

We now set $\varphi = \theta_{\text{ML}}^{(m)}$. Since this phase maximizes \mathcal{L} , the left-hand-side vanishes and we obtain

$$(\theta_{\text{ML}}^{(m)} - \theta) \simeq -\frac{\partial_\varphi \log \mathcal{L}(\varphi)|_\theta}{\partial_\varphi^2 \log \mathcal{L}(\varphi)|_\theta}. \quad (\text{A.7})$$

The consistency of the estimator ensures that we can neglect terms of higher order in $\theta_{\text{ML}}^{(m)} - \theta$ provided that m is large enough.

In order to investigate how $\theta_{\text{ML}}^{(m)} - \theta$ is distributed, we start by computing the average of the denominator,

$$\begin{aligned} \partial_\varphi^2 \log \mathcal{L}(\varphi)|_\theta &= m \left[\frac{1}{m} \sum_{i=1}^m \sum_{k=1}^N \partial_\varphi^2 \log (p_1(x_k^{(i)}|\varphi)) \Big|_\theta \right] \\ &\rightarrow_{m \gg 1} m \sum_{k=1}^N \int d\vec{x}_N p_N(\vec{x}_N|\theta) \partial_\varphi^2 \log (p_1(x_k|\varphi)) \Big|_\theta \\ &= -mNF_1. \end{aligned} \quad (\text{A.8})$$

The coefficient N results from the indistinguishability of the particles and F_1 is the Fisher information calculated with the single particle probability density,

$$F_1 = \int dx_1 \frac{1}{p(x_1|\theta)} (\partial_\varphi p(x_1|\varphi)|_\theta)^2. \quad (\text{A.9})$$

Coming back to Eq. (A.7), we get

$$(\theta_{\text{ML}}^{(m)} - \theta) \simeq \frac{1}{m} \sum_{i=1}^m \left[\frac{1}{NF_1} \sum_{k=1}^N \partial_\varphi \log (p_1(x_k^{(i)}|\varphi)) \Big|_\theta \right]. \quad (\text{A.10})$$

Hence the difference $\theta_{\text{ML}}^{(m)} - \theta$ is the average of m random variables, which in the central limit are distributed with a Gaussian probability. With a calculation similar to the one of Eq. (A.8) one obtains that the average value vanishes, which means that the MLE is *unbiased*. The variance of the distribution in the central limit is

$$\Delta^2 \theta_{\text{ML}}^{(m)} = \frac{1}{m} \frac{1}{NF_1} \left(1 + (N-1) \frac{C}{F_1} \right) \quad (\text{A.11})$$

where

$$C = \int dx_1 dx_2 p_2(x_1, x_2|\theta) \frac{\partial_\theta p_1(x_1|\theta)}{p_1(x_1|\theta)} \frac{\partial_\theta p_1(x_2|\theta)}{p_1(x_2|\theta)}. \quad (\text{A.12})$$

Therefore the Fisher information from Eq. (A.1) is

$$F = \frac{NF_1}{\left(1 + (N-1) \frac{C}{F_1} \right)}. \quad (\text{A.13})$$

Hence the correlations enter *via* the two-particle correlation function p_2 even though in the definition of the estimator only the single body density p_1 is used.

Appendix A.2. Multiple-atom detection

The multiple-atom detection relies upon dividing the space into n_{bin} bins, each of size Δx . In every bin, the number of atoms is measured and this result is averaged over m realizations, giving

$$\bar{n}_k = \frac{1}{m} \sum_{i=1}^m n_k^{(i)}. \quad (\text{A.14})$$

According to the central limit theorem, for large m the probability of detecting \bar{n}_k is Gaussian,

$$p(\bar{n}_k|\varphi) = \frac{1}{\sqrt{2\pi\Delta^2 n_k/m}} e^{-\frac{(\bar{n}_k - \langle n_k \rangle)^2}{2\Delta^2 n_k/m}}. \quad (\text{A.15})$$

Here, $\langle n_k \rangle = \lim_{m \rightarrow \infty} \bar{n}_k$ and $\Delta^2 n_k$ are the associated fluctuations and both depend on the value of φ . We construct the likelihood function as follows

$$\mathcal{L}_{\text{fit}}(\varphi) = \prod_{k=1}^{n_{\text{bin}}} p(\bar{n}_k|\varphi). \quad (\text{A.16})$$

Again, we follow the steps of the proof of Fisher's theorem and expand the derivative of the logarithm of the likelihood function around the true value and set $\varphi = \theta_{\text{ML}}^{(m)}$,

$$(\theta_{\text{ML}}^{(m)} - \theta) \simeq -\frac{\partial_\varphi \log \mathcal{L}_{\text{fit}}(\varphi)|_\theta}{\partial_\varphi^2 \log \mathcal{L}_{\text{fit}}(\varphi)|_\theta}. \quad (\text{A.17})$$

For the following calculations we introduce the more compact notation

$$\partial_\varphi u(\varphi)|_\theta \equiv \partial_\theta u, \quad (\text{A.18})$$

used also in the main text. We start with calculating the denominator of Eq. (A.17) which in the large m limit reads,

$$\begin{aligned} \partial_\theta^2 \log \mathcal{L}_{\text{fit}} &= -m \sum_{k=1}^{n_{\text{bin}}} \left[\frac{(\partial_\theta \langle n_k \rangle)^2}{\Delta^2 n_k} + [\langle n_k \rangle - \bar{n}_k] \left(\frac{\partial_\theta^2 \langle n_k \rangle}{\Delta^2 n_k} + \partial_\theta \langle n_k \rangle \partial_\theta \frac{1}{\Delta^2 n_k} \right) \right. \\ &\quad \left. + \frac{1}{2} [\bar{n}_k - \langle n_k \rangle]^2 \partial_\theta^2 \frac{1}{\Delta^2 n_k} \right]. \end{aligned} \quad (\text{A.19})$$

According to (A.18), both $\langle n_k \rangle$ and $\Delta^2 n_k$ in the above equation are a function of θ . In analogy to Eq. (A.8) for $m \rightarrow \infty$ above denominator is replaced with its average value. Upon averaging, the second term vanishes and the third term is proportional to $\Delta^2 n_k/m$, which is negligible in the limit of large m . Therefore we obtain

$$\partial_\theta^2 \log \mathcal{L}_{\text{fit}} \simeq -m \sum_{k=1}^{n_{\text{bin}}} \frac{(\partial_\theta \langle n_k \rangle)^2}{\Delta^2 n_k}. \quad (\text{A.20})$$

The average of the square of the nominator of Eq. (A.17) reads

$$\begin{aligned}
\langle (\partial_\theta \log \mathcal{L}_{\text{fit}})^2 \rangle &\simeq m^2 \sum_{k,l=1}^{n_{\text{bin}}} \frac{\partial_\theta \langle n_k \rangle \partial_\theta \langle n_l \rangle}{\Delta^2 n_k \Delta^2 n_l} \langle (\bar{n}_k - \langle n_k \rangle)(\bar{n}_l - \langle n_l \rangle) \rangle \\
&- 2m^2 \sum_{k,l=1}^{n_{\text{bin}}} \frac{\partial_\theta \langle n_k \rangle}{\Delta^2 n_k} \partial_\theta \frac{1}{2\Delta^2 n_l} \langle (\bar{n}_k - \langle n_k \rangle)(\bar{n}_l - \langle n_l \rangle)^2 \rangle \\
&+ m^2 \sum_{k,l=1}^{n_{\text{bin}}} \partial_\theta \frac{1}{2\Delta^2 n_k} \partial_\theta \frac{1}{2\Delta^2 n_l} \langle (\bar{n}_k - \langle n_k \rangle)^2 (\bar{n}_l - \langle n_l \rangle)^2 \rangle.
\end{aligned} \tag{A.21}$$

The second term vanishes and the last, after the average is calculated in the central limit, becomes m -independent, and thus can be dropped when compared to the first term.

Let us now separate the sum over k, l into $k = l$ and $k \neq l$ parts. The first one simply gives

$$m \sum_{k=1}^{n_{\text{bin}}} \frac{(\partial_\theta \langle n_k \rangle)^2}{\Delta^2 n_k}. \tag{A.22}$$

The non-diagonal part $k \neq l$ depends on the two-site correlations $\sigma_{kl}^2 = m \langle (\bar{n}_k - \langle n_k \rangle)(\bar{n}_l - \langle n_l \rangle) \rangle$. To justify Eq. (5) of the main text, we notice that the atom-number fluctuations read

$$\Delta^2 n_k = p_1(x_k|\theta)\Delta x + (p_2(x_k, x_k|\theta) - p_1(x_k|\theta)^2)(\Delta x)^2 \tag{A.23}$$

and thus in a small bin-size limit are Poissonian, i.e. $\Delta^2 n_k = p_1(x_k|\theta)\Delta x = \langle n_k \rangle$. Therefore,

$$\Delta^2 \theta_{\text{fit}}^{(m)} = \frac{\sum_{k=1}^{n_{\text{bin}}} \frac{[\partial_\theta \langle n_k \rangle]^2}{\langle n_k \rangle} + \sum_{k \neq l=1}^{n_{\text{bin}}} \sigma_{k,l}^2 \frac{\partial_\theta \langle n_k \rangle}{\langle n_k \rangle} \frac{\partial_\theta \langle n_l \rangle}{\langle n_l \rangle}}{m \left[\sum_{k=1}^{n_{\text{bin}}} \frac{[\partial_\theta \langle n_k \rangle]^2}{\langle n_k \rangle} \right]^2}. \tag{A.24}$$

The last step is to calculate the cross-correlation term

$$\begin{aligned}
\sigma_{k,l}^2 &= (\Delta x)^2 \left[\langle \hat{\Psi}^\dagger(x_k|\theta) \hat{\Psi}(x_k|\theta) \hat{\Psi}^\dagger(x_l|\theta) \hat{\Psi}(x_l|\theta) \rangle - \langle \hat{\Psi}^\dagger(x_k|\theta) \hat{\Psi}(x_k|\theta) \rangle \langle \hat{\Psi}^\dagger(x_l|\theta) \hat{\Psi}(x_l|\theta) \rangle \right] \\
&= (\Delta x)^2 N [(N-1)p_2(x_k, x_l|\theta) - Np_1(x_k|\theta)p_1(x_l|\theta)],
\end{aligned}$$

where in the last line we used

$$\begin{aligned}
\langle \hat{\Psi}^\dagger(x_k|\theta) \hat{\Psi}(x_k|\theta) \hat{\Psi}^\dagger(x_l|\theta) \hat{\Psi}(x_l|\theta) \rangle &= \\
\langle \hat{\Psi}^\dagger(x_k|\theta) \hat{\Psi}^\dagger(x_l|\theta) \hat{\Psi}(x_l|\theta) \hat{\Psi}(x_k|\theta) \rangle &= N(N-1)p_2(x_k, x_l|\theta),
\end{aligned} \tag{A.25}$$

which is true for $k \neq l$.

Appendix B. Derivation of the phase uncertainty for the MZI

When the two wave-packets are fully separated, so that $\psi_a(x)\psi_b(x) = 0$ for all x , the one-body probability reads

$$p_1(x|\theta) = \frac{1}{N} \langle \hat{\Psi}^\dagger(x|\theta) \hat{\Psi}(x|\theta) \rangle = \frac{1}{2} [|\psi_a(x)|^2(1 - \nu \sin \theta) + |\psi_b(x)|^2(1 + \nu \sin \theta)],$$

where $\nu = \frac{2}{N}\langle \hat{J}_x \rangle$ is the fringe visibility. This probability gives

$$\begin{aligned} F_1 &= \int dx \frac{[\partial_\theta p_1(x|\theta)]^2}{p_1(x|\theta)} = \frac{\nu^2 \cos^2 \theta}{2} \int dx \frac{|\psi_a(x)|^4 + |\psi_b(x)|^4}{|\psi_a(x)|^2(1 - \nu \sin \theta) + |\psi_b(x)|^2(1 + \nu \sin \theta)} \\ &= \frac{\nu^2 \cos^2 \theta}{1 - \nu^2 \sin^2 \theta}. \end{aligned}$$

Now we calculate the second order probability and get [cf. Eq. (4)]

$$\begin{aligned} N(N-1)p_2(x_1, x_2|\theta) &= \langle \hat{\Psi}^\dagger(x_1|\theta)\Psi^\dagger(x_2|\theta)\hat{\Psi}(x_2|\theta)\hat{\Psi}(x_1|\theta) \rangle = \frac{N^2}{2} (|\psi_a(x_1)|^2 + |\psi_b(x_1)|^2)p_1(x_2) \\ &+ (|\psi_a(x_1)|^2 - |\psi_b(x_1)|^2)(|\psi_a(x_2)|^2 - |\psi_b(x_2)|^2) \left[\cos^2 \theta \left(\langle \hat{J}_z^2 \rangle - \frac{N}{4} \right) + \sin^2 \theta \left(\langle \hat{J}_x^2 \rangle - \frac{N}{4} \right) \right] \\ &+ (|\psi_b(x_1)|^2 - |\psi_a(x_1)|^2)(|\psi_a(x_2)|^2 + |\psi_b(x_2)|^2) \frac{N}{2} \sin \theta \langle \hat{J}_x \rangle. \end{aligned}$$

We insert this function together with $p_1(x|\theta)$ into the definition of C and obtain

$$\begin{aligned} N(N-1) \cdot C &= \frac{N^2}{4} (\alpha + \beta)^2 + \left(N - \frac{1}{2} \right) \langle \hat{J}_x \rangle (\beta^2 - \alpha^2) \sin \theta \\ &+ \left(\langle \hat{J}_z^2 \rangle \cos^2 \theta + \langle \hat{J}_x^2 \rangle \sin^2 \theta - \frac{N}{4} \right) (\alpha - \beta)^2, \end{aligned}$$

where

$$\alpha = -\frac{\langle \hat{J}_x \rangle \cos \theta}{\frac{N}{2} - \langle \hat{J}_x \rangle \sin \theta} \quad \text{and} \quad \beta = \frac{\langle \hat{J}_x \rangle \cos \theta}{\frac{N}{2} + \langle \hat{J}_x \rangle \sin \theta}. \quad (\text{B.1})$$

If we now combine expressions for F_1 and C as in Eq. (3), we obtain Eq. (9).

Appendix C. The one- and two-body probabilities for the interference pattern

The explicit expression for the one-body probability comes directly from the definitions of $p_1(x|\theta)$ and the angular momentum operators,

$$p_1(x|\theta) = \frac{1}{N} \langle \hat{\Psi}^\dagger(x|\theta)\hat{\Psi}(x|\theta) \rangle = \left| \tilde{\psi} \left(\frac{x}{\tilde{\sigma}^2} \right) \right|^2 \left(1 + \frac{2\langle \hat{J}_x \rangle}{N} \cos(\kappa x + \theta) \right). \quad (\text{C.1})$$

Clearly, the coefficient $\nu \equiv \frac{2\langle \hat{J}_x \rangle}{N}$ is the visibility of the interference fringes. The two body probability reads [cf. Eq. (4)]

$$\begin{aligned} p_2(x_1, x_2|\theta) &= \frac{\langle \hat{\Psi}^\dagger(x_1|\theta)\Psi^\dagger(x_2|\theta)\hat{\Psi}(x_2|\theta)\hat{\Psi}(x_1|\theta) \rangle}{N(N-1)} = \left| \tilde{\psi} \left(\frac{x_1}{\tilde{\sigma}^2} \right) \right|^2 \left| \tilde{\psi} \left(\frac{x_2}{\tilde{\sigma}^2} \right) \right|^2 \times \\ &\times \left[1 - \frac{1}{(N-1)} \cos(\kappa(x_1 - x_2)) + \frac{2\langle \hat{J}_x \rangle}{N} [\cos(\kappa x_1 + \theta) + \cos(\kappa x_2 + \theta)] \right. \\ &\left. + \frac{4\langle \hat{J}_z^2 \rangle}{N(N-1)} \cos(\kappa x_1 + \theta) \cos(\kappa x_2 + \theta) + \frac{4\langle \hat{J}_x^2 \rangle}{N(N-1)} \sin(\kappa x_1 + \theta) \sin(\kappa x_2 + \theta) \right]. \quad (\text{C.2}) \end{aligned}$$

Appendix D. Gaussian scaling

To find the best possible scaling of the phase uncertainty (12) with N , we model $|\psi_{\text{in}}\rangle$ with a Gaussian state as follows

$$|\psi_{\text{in}}\rangle \propto e^{-i\frac{\pi}{2}\hat{J}_x} \sum_j e^{-\frac{(j-\frac{N}{2})^2}{N\cdot\xi_\phi}} |j, N-j\rangle. \quad (\text{D.1})$$

The operator $e^{-i\frac{\pi}{2}\hat{J}_x}$ represents a beam-splitter which transforms the number- to the phase-squeezed state. For $\xi_\phi = 1$ the resulting state is spin-coherent, and by decreasing ξ_ϕ we increase the amount of phase-squeezing.

This state is used to calculate the expectation values $\langle\hat{J}_x\rangle$ and $\langle\hat{J}_y^2\rangle$ from Eq. (12). For $N \gg 1$ the summation over j can be approximated with an integral. This way we obtain analytical expressions

$$\langle\hat{J}_x\rangle^2 = \frac{N^2}{4} e^{-\frac{1}{N\cdot\xi_\phi}} \quad \text{and} \quad \langle\hat{J}_y^2\rangle = \frac{N^2}{8} \left(1 - e^{-\frac{2}{N\cdot\xi_\phi}}\right). \quad (\text{D.2})$$

which are then substituted into Eq. (12). Taking $\xi_\phi = N^{-\beta}$, where $0 \leq \beta \leq 1$, we get

$$m\Delta^2\theta_{\text{ML}}^{(m)} = N^{-(\beta+1)} + N^{\frac{\beta-3}{2}}. \quad (\text{D.3})$$

The phase uncertainty is optimal, when these two terms are equal, otherwise one of them would dominate at large N . This condition gives $\beta^{\text{opt}} = \frac{1}{3}$ and $m\Delta^2\theta_{\text{ML}}^{(m),\text{opt}} = 2N^{-4/3}$.

References

- [1] Giovanetti V, Lloyd S and Maccone L 2004 *Science* **306** 1330
- [2] Mitchell M W, Lundeen J S and Steinberg A M 2004 *Nature* **429** 726
- [3] Walther P, Pan J-W, Aspelmeyer M, Ursin R, Gasparoni S and Anton Zeilinger 2004 *Nature* **429** 158
- [4] Afek I, Ambar O and Y. Silberberg 2010 *Science* **328** 879
- [5] Kacprowicz M, Demkowicz-Dobrzański R, Wasilewski W, Banaszek K and Walmsley I A 2010 *Nat. Photonics* **4** 357
- [6] Leibfried D, Barrett M D, Schaetz T, Britton J, Chiaverini J, Itano W M, Jost J D, Langer C and Wineland D J 2004 *Science* **304** 1476
- [7] Appel J, Windpassinger P J, Oblak D, Hoff U B, Kjørgaard N and Polzik E S 2009 *PNAS* **106** 10960
- [8] Schleier-Smith M H, Leroux I D and Vuletić V 2010 *Phys. Rev. Lett.* **104** 073604
- [9] Gross C, Zibold T, Nicklas E, Estève and Oberthaler M K 2010 *Nature* **464** 1165
- [10] Estève, Gross C, Weller A, Giovanazzi S and Oberthaler M K 2008 *Nature* **455** 1216
- [11] Riedel M F, Böhi P, Li Y, Hänsch T W, Sinatra A and Treutlein P 2010 *Nature* **464** 1170
- [12] Maussang K, Marti G E, Schneider T, Treutlein P, Li Y, Sinatra A, Long R, Estève J Reichel J 2010 *Phys. Rev. Lett.* **105** 080403
- [13] Cronin A D, Schmiedmayer J and Pritchard D E 2009 *Rev. Mod. Phys.* **81** 1051
- [14] Pasquini T A, Shin Y, Sanner C, Saba M, Schirotzek A, Pritchard D E and Ketterle W 2004 *Phys. Rev. Lett.* **93** 223201
- [15] Lin Yu-ju, Teper I, Chin Ch and Vuletić V 2004 *Phys. Rev. Lett.* **92** 050404
- [16] Obrecht J M, Wild R J, Antezza M, Pitaevskii L P, Stringari S and Cornell E. A. 2007 *Phys. Rev. Lett.* **98** 063201
- [17] Anderson B P and Kasevich M A 1998 *Science* **282** 1686

- [18] Fattori M, D'Errico C, Roati G, Zaccanti M, Jona-Lasinio M, Modugno M, Inguscio M and Modugno G 2008 *Phys. Rev. Lett.* **100** 080405
- [19] Baumgärtner, Sewell R J, Eriksson S, Llorente-Garcia I, Dingjan J, Cotter J P and Hinds E A 2010 *Phys. Rev. Lett.* **105** 243003
- [20] Wineland D J, Bollinger J J, Itano W M and Heinzen D J 1994 *Phys. Rev. A* **50** 67
- [21] Pezzé L, Smerzi A, Berman G P, Bishop A R and Collins L A 2006 *Phys. Rev. A* **74** 033610
- [22] Grond J, Hohenester U, Schmiedmayer J and Smerzi A 2011 *Phys. Rev. A* **84** 023619
- [23] Jelte T *et al.* 2007 *Nature* **445** 402
- [24] Heine D, Rohringer W, Fischer D, Wilzbach M, Raub T, Loziczky S, Liu XiYuan, Groth S, Hessmo B and Schmiedmayer J 2010 *New J. Phys.* **12** 095005
- [25] Bücker, Perrin A, Manz S, Betz T, Koller Ch, Plisson T, Rottmann J, Schumm T and Schmiedmayer J 2009 *New J. Phys.* **11** 103039
- [26] Sherson J F, Weitenberg C, Endres M, Cheneau M, Bloch I and Kuhr S 2010 *Nature* **467** 68
- [27] Chwedeńczuk J, Piazza F and Smerzi A 2010 *Phys. Rev. A* **82** 051601(R)
- [28] Chwedeńczuk J, Piazza F and Smerzi A 2011 *New J. Phys.* **13** 065023
- [29] Chwedeńczuk J, Pezzé L, Piazza F and Smerzi A 2010 *Phys. Rev. A* **82** 032104
- [30] We use an abbreviated notation for the derivatives, $\partial_\theta f = \partial_\theta f(\theta) \equiv [\partial_\varphi f(\varphi)]|_{\varphi=\theta}$.
- [31] The angular momentum operators are $\hat{J}_x \equiv (\hat{a}^\dagger \hat{b} + \hat{b}^\dagger \hat{a})/2$, $\hat{J}_y \equiv (\hat{a}^\dagger \hat{b} - \hat{b}^\dagger \hat{a})/2i$ and $\hat{J}_z \equiv (\hat{a}^\dagger \hat{a} - \hat{b}^\dagger \hat{b})/2$.
- [32] Kitagawa M and Ueda M 1993 *Phys. Rev. A* **47** 5138
- [33] Pezzé L and Smerzi A 2009 *Phys. Rev. Lett.* **102** 100401
- [34] Masiello D J and Reinhardt W P, *Phys. Rev. A* **76** 043612 (2007)
- [35] Cederbaum L S, Streltsov A I, Band Y B and Alon O E, *Phys. Rev. Lett.* **98**, 110405 (2007)
- [36] Grond J, Hohenester U, Mazets I and Schmiedmayer J 2010 *New J. Phys.* **12** 065036
- [37] Braunstein S L and Caves C M 1994 *Phys. Rev. Lett.* **72** 3439
- [38] Lücke B *et al.* 2011 *Science* **334** 773
- [39] Cramér H 1946 *Mathematical Methods of Statistics*, (Princeton Univ. Press, Princeton, NJ)
- [40] Ferguson T S 1996 *A Course in Large Sample Theory*, (Chapman & Hall, London, UK)
- [41] Barlow R J 1989 *A Guide to the Use of Statistical Methods in the Physical Sciences*, (Wiley, Chichester, UK)